Joint 48th IEEE Conference on Decision and Control and
28th Chinese Control Conference
Shanghai, P.R. China, December 16-18, 2009

Nonparametric Density Estimation of Bubble Size Distribution for Monitoring Mineral Flotation Process

Chunhua Yang, Canhui Xu, Weihua Gui, and Jianjiang Du

Abstract— **The mineral separation efficiency of flotation process depends very much on the surface properties of feed ore and addition of chemical reagents. Machine vision based analysis of froth appearance is considered as an indication of flotation performance. Bubble structure obtained by watershed segmentation scheme is used to determine the amount of reagent. To explore bubble size distribution, nonparametric wavelet thresholding estimator is introduced to approximate the output Probability Density Function (PDF). With the aim of tracking the output PDFs to a target distribution shape, the output PDF model is therefore transformed into the dynamic weight coefficients model which allows a predicted reagent addition profile to be identified for controlling the flotation process.**

I. INTRODUCTION

As the increasing consumption of the scarce mineral resource, flotation is becoming an indispensable technology to effectively utilize the low-graded ore resources. It aims to separate valuable minerals from useless materials or other minerals through complex physiochemical processes. By the addition of chemicals and mixture of air, valuable minerals are made hydrophobic in order to attach to the air bubbles, which rise up to the froth layer on the top of slurry where the upgraded valuable minerals are collected.

It is well recognized that flotation process is a multivariate complex process influenced by various factors, and the control and modeling are very challenging. Currently, the manipulation of flotation process depends heavily on human operators to observe and interpret the visual appearance of the froth, so as to estimate the process condition using their experience in the field. This empirical approach is subjective, and prone to failure, mainly because the human vision is limited in terms of its distinguishing ability and accuracy. Recent advances in image processing and computer vision provide new opportunities to gain a better understanding of the industrial flotation process through monitoring froth appearances [1].

Numerous reported literatures focus their attention on the extraction techniques of froth features such as texture color [2], bubble size [3], froth speed [4] and bubble load [5]. It is believed that operating process status can be characterized by bubble structure, which is used by human operators as heuristic knowledge. O' Conner et al [6] reported that increase in pH causes bubble size to increase, consequently, the variance of bubble size has great effect on the probability of collision between mineral particles and bubbles, as well as the adhesion of these particles to the bubbles. Moolman [1] claimed that the result is consistent with the observation in the case of pyrite, and the mineral recovery decreased at higher pH. Approaches reported to segment the froth images and estimate bubble size, include white spots detection [7], watershed method [8], wavelet transformation [9], valley edge detection and their varieties [10]. Further analyses on the segmented froth images are confined to calculate average bubble size or determine other characteristics like mean, variance, kurtosis, and skewness, except that Liu described the size distribution by classifying them into three groups: large, middle and small size [9]. A more recent flotation control proposed by Liu is based on the wavelet size signature using linear scale continuous wavelet transform (CWT) [11]. Even though the size distribution is of great significance, the information indicated by statistical size distribution is far from fully utilized.

Regarding the density distribution, nonparametric estimation is one of the core operations to analyze the unknown continuous process. Wavelet estimation tends to stand out other most commonly used methods such as histogram, kernel estimators for its ability to identify discontinuities as well as local oscillations [14].

This work aims to thoroughly explore the froth structure by using wavelet-based density estimation technique to approximate the output probability density function (PDF) of bubble size distribution. Segmentation results of the on-line acquired froth images using the watershed method can subsequently be processed to estimate the PDF of bubble size distribution. By estimating the PDF of bubble size distribution, tracking of size density is reduced to monitoring the wavelet coefficients vector, which can directly be related to operational variables, such as chemical reagent addition. The next section introduces bubble characteristic oriented watershed segmentation scheme, Section 3 presents the nonparametric density estimation and nonlinear wavelet density estimators. Section 4 presents the experimental results and discussion. Conclusion is provided in the last section.

II. FROTH SEGMENTATION

The most important step in froth image analysis is to delineate every bubble. As mentioned earlier, the segmentation methodology varies from one to another.

This work was supported by the Key Program of National Natural Science of China under Grant No. 60634020, the National Natural Science Foundation of China under Grant No. 60874069 and 863 Program of China under Grant No. 2006AA04Z181.

Chunhua Yang, Canhui Xu, Weihua Gui and Jianjiang Du are in the School of Information Science and Engineering, Central South University, Changsha 410083, China. (e-mails: {ychh, christinexu, gwh }@mail.csu.edu.cn).

Considering the characteristics of froth images collected from industry field, which show that: (1) a froth image is fully occupied by bubbles, in normal cases, without gaps or background region between bubbles; (2) the illumination on bubble surface is uneven; (3) each bubble has a convex shape which leads to the appearance of white spots, generally on the top if the incident ray is right from the vertical direction of froth layer; (4) edges between bubbles are weak, while edges caused by spot highlight are obvious; the edge between bubbles can hardly be detected by using classical edge detector. In contrast, the boundaries between bubbles are weak, with lower gradient magnitude, some of which are local minimum intensity of the cross section of froth images. A detection scheme, Valley Edge Detection based segmentation (VED) would be suitable to avoid strong edges around the white spots [10]. But its segmentation results will make the probability of size distribution not sum up to one, which limits its application in this work. Among the reported image segmentation methodologies, watershed method is another good alternative [8].

The idea of watershed is based on simulating water flows in a topographic representation of image intensity. As shown in Fig.1, a three dimensional landscape can describe the topography, which consists of valleys and hills, representing the lower and higher intensity of an image respectively. Suppose that a hole is punched in each regional minimum. Put the model into a lake. Then water is immersed from the bottom through the hole at a uniform rate. When two lakes meet, the watershed can be identified. The flooding will eventually be accomplished until the entire landscape has been fully immersed.

The principal objective is to find the watershed lines where the borders separate valleys belonging to different local minima. Direct application of the watershed transform usually leads to oversegmentation. Marker-Controlled Watershed Segmentation is applied to solve the

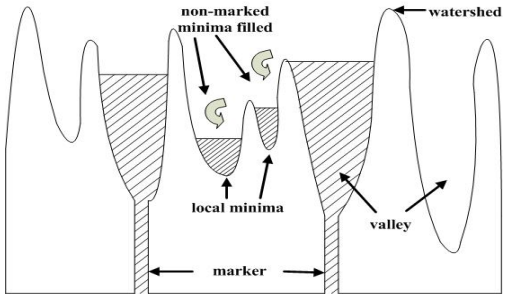

Fig. 1. Immersion from marked to non-marked area.

oversegmentation problem. A preprocessing step is incorporated by using makers bringing a priori knowledge before watershed transform. In practical setup, the spotlights reflected on each bubble are used as makers. The h-dome transform is used to extract light structures, i.e. regions of pixels which are brighter than their immediate surroundings. An h-dome D of image X is defined as a connected component of pixels such that every pixel p that is a neighbor of D satisfies:

$$\begin{cases} X(p) < \min\{X(q) \mid q \in D\} \\ \max\{X(q) \mid q \in D\} - \min\{X(q) \mid q \in D\} < h \end{cases} \quad (1)$$

Consequently, the value of a pixel p in the h-dome D is:

$$X(p) - \min\{X(q) \mid q \in D\} \quad (2)$$

which means the pixel values are offset at the minimum intensity value of the h-dome. In fact, the h-dome extraction is based on a process called grey-scale reconstruction, which is implemented by using iterated grey-scale dilations and infimums. After the maker extraction, watershed segmentation can proceed automatically.

Online videos and froth images with the size of 800×600 are recorded by a RGB camera over the flotation rougher cell in a flotation industry field of China since July, 2008. The segmentation results of three typical images, which are collected under the same condition (resolution, angle, light condition, position, view scale, etc.) but at different time, are presented in Fig.2. For human vision, these images are visually discriminative in terns of color and bubble structure. The color textural information of bubbles in the rougher cell

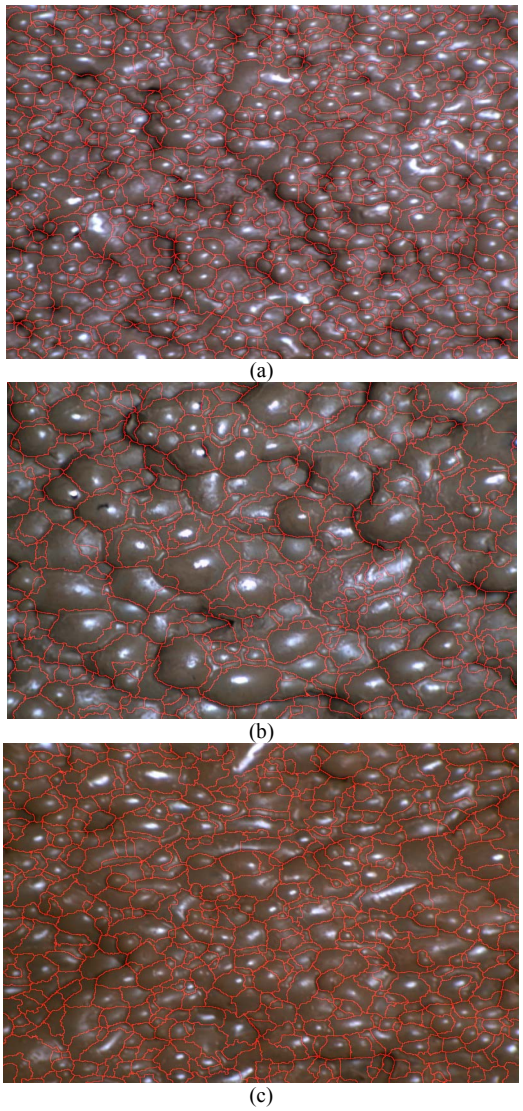

(a) (b) (c)

Fig.2 Segmentation results of typical froth images: (a) froth type 1, (b) froth type 2 and (c) froth type 3.

is directly related to the grade of ore feed, which is a dominant factor affecting the flotation performance. On the other hand, the bubble structures are an indication of chemical addition, which is determinant to mineral separation efficiency. Small bubbles with relative maximum surface area generally carry more valuable mineral particles, whose corresponding pH value is confined to an ideal bounded range (normally 9.6~9.8). As is shown in Fig.2 (a), the froth structure is sticky and bubbles are averagely small and with spherical shapes. The calculated total bubble number is 836 with average area of 514 pixels, and its corresponding pH value is 9.75. The froth structure in Fig.2 (b) is mostly round and with large size. Due to the excessive addition of activator Na_2Co_3, pH value rose up to 10, far beyond the normal range. The calculated total bubble number is 439 with average area of 1009 pixels. In Fig.2(c), in the case of ore feed interrupting period; the flow rate of activator Na_2Co_3 was slowing down, therefore, the pH value decreased to about 9.45, lower than normal value; the calculated total bubble number is 544 with average area of 803 pixels .

III. NONPARAMETRIC WAVELET ESTIMATION

With the segmentation results obtained, the real-time data analysis and status monitoring is the next priority. Nonparametric density estimation has the desired property of capturing an unknown distribution of a continuous process, such as the segmentation results of the images for the bubble size distribution.

To describe the dynamic stochastic process, let $y(t) \in (a,b)$ be the bounded output of the system the probability, $u(t) \in R^m$ the control input dominating the output PDF shape of $y(t)$. The conditional probability of output $y(t)$ lying inside $[a,\xi]$ is defined as:

$$P(a \le y(t) < \xi) = \int_a^{\xi} \gamma(v,u(t))dv \qquad (3)$$

where $\gamma(v,u(t))$ is the conditional output PDF. To approximate $\gamma(v,u(t))$, many papers in literature have been devoted to the nonparametric estimation, including kernel methods, orthogonal methods, the histogram and their varieties [12]. More recently, Wang et al proposed the B-spline expansion models that successfully tracked the output PDFs to a target distribution shape by using various control approaches [13].

Considering the characteristics of the size distribution of froth segmentation results, it is shown that the output PDF is smooth but with spikes, with an obvious long tail skewed to the left. Kernel methods generally tend to underestimate the peaks of discrete sampling density and so will bias the likelihood ratio [14]. Unlike other estimators, wavelets are orthogonal bases of function spaces with many appealing properties like representing the discontinuities, local oscillations and spikes. And it is reported that wavelet estimators tend to be superior to other estimation techniques [15].

The basic scheme of wavelet expansion of the output probability density function $\gamma(x)$ is:

$$\gamma(x) \sim \sum_k c_{j_1,k}\phi_{j_1,k}(x) + \sum_{j>j_1}\sum_k d_{j,k}\psi_{j,k}(x) \qquad (4)$$

where coefficients $c_{j_1,k}$ and $d_{j,k}$ are given as:

$$c_{j_1,k} = \int_{-\infty}^{+\infty} \phi_{j_1,k}\gamma(x)dx \,,\; d_{j,k} = \int_{-\infty}^{+\infty} \psi_{j,k}\gamma(x)dx \,.$$

Wavelet basis is derived from the scaling function $\phi_{j_1,k}(x) = 2^{j_1/2}\phi(2^{j_1}x-k), k \in \mathbb{Z}$ and the mother wavelet $\psi_{j,k}(x) = 2^{j/2}\psi(2^j x-k), k \in \mathbb{Z}, j > j_1$, where j is the resolution parameter, k is the translation parameter. For general orthogonal series estimators, empirical wavelet coefficients can be formed as:

$$\hat{c}_{j_1,k} = \frac{1}{n}\sum_{i=1}^{n}\phi_{j_1,k}(X_i) \qquad (5)$$

$$\hat{d}_{j,k} = \frac{1}{n}\sum_{i=1}^{n}\psi_{j,k}(X_i) \qquad (6)$$

Replace (4) with the unbiased estimate $\hat{c}_{j_1,k}$ and $\hat{d}_{j,k}$. Obviously $\gamma(x)$ is approximated by a linear wavelet estimator, linear combinations of scaling function and mother wavelet. To automatically adapt to local features of a density, Donoho [16] developed nonlinear wavelet estimator by thresholding empirical coefficients

$$\tilde{d}_{j,k} = \delta(\hat{d}_{j,k},\lambda_j), \delta = \delta_s, \delta_h \qquad (7)$$

where $\delta_s(\hat{d}_{j,k},\lambda) = \operatorname{sgn}\hat{d}_{j,k}(\hat{d}_{j,k}-\lambda)_+$ indicates soft thresholding shrinking large coefficients to zero, hard thresholding $\delta_h(\hat{d}_{j,k},\lambda) = \hat{d}_{j,k}I\{|\hat{d}_{j,k}| > \lambda\}$ sets coefficients with absolute value larger than λ to zero. By choosing the appropriate thresholding parameter λ for each resolution j. Then (4) becomes

$$\tilde{\gamma}(x) \sim \sum_k c_{j_1,k}\phi_{j_1,k}(x) + \sum_{j>j_1}\sum_k \tilde{d}_{j,k}\psi_{j,k}(x) \qquad (8)$$

It is shown in [16] that the convergence rate of nonlinear wavelet threshold estimators are generally faster than linear wavelet estimators.

IV. EXPERIMENTAL RESULTS AND DISCUSSION

In this work, near symmetric wavelets 'sym4' designed by Daubechies [17] is applied, which are compactly supported wavelets with least amount of asymmetry and highest number of vanishing moments for a given support width. Associated scaling filters are near linear-phase filters (shown in Fig.3). j_1 is selected according to the regularity of the function,

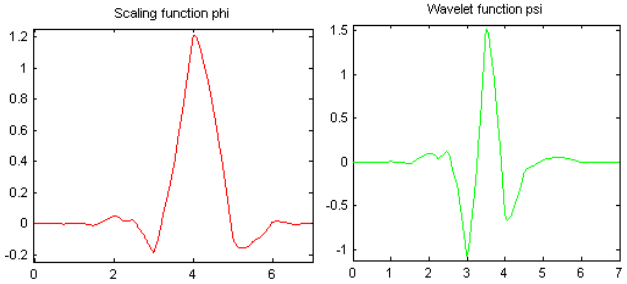

Fig.3 Scaling and wavelet function of 'sym4'.

$j = \lfloor \log_2 n - \log_2(\log n) \rfloor$, and a scale dependent thresholding $\lambda_j = C\sqrt{j/n}$ with an appropriate constant C is selected [16]. Take the segmented image Fig.2(c) as an example, the total number of bubbles are 544, with an average area 803 pixels (inside each bubble), the average length (in pixels) of the major axis of the ellipse is 42 and the average length (in pixels) of the minor axis of the ellipse is 24. A histogram with 64 bins is used. Nonparametric nonlinear wavelet estimator proposed in section 3 is then applied to approximate the size probability density, which is heavily skewed to the left. As is shown in Fig.4, the histogram display

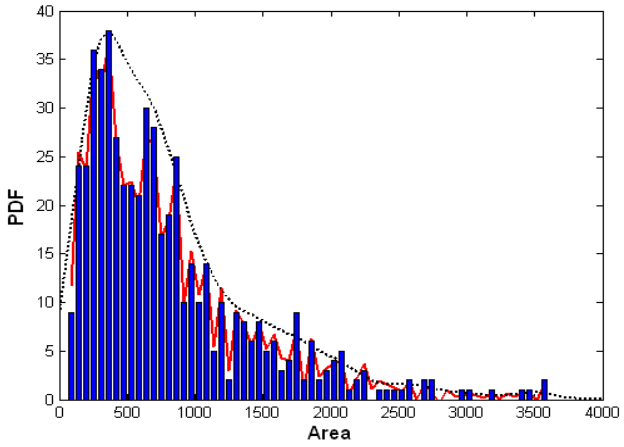

Fig.4 Nonparametric estimation of bubble size density.

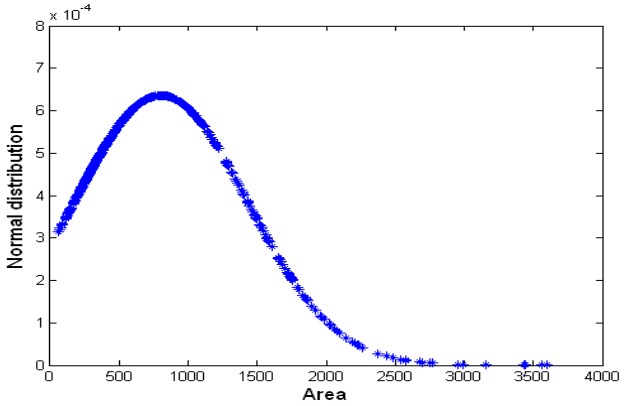

Fig.5 Normal distribution regression.

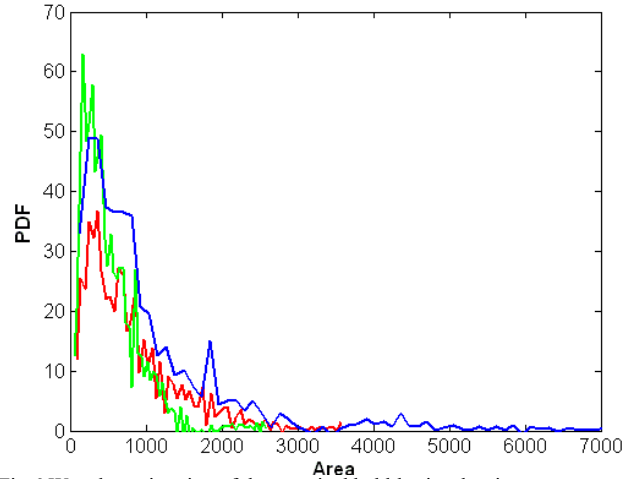

Fig.6 Wavelet estimation of three typical bubble size density.

of froth image Fig.2(c) is illustrated, the red solid line represents the estimation result of wavelet expansion, which accurately approximates the size density distribution as expected. For comparison reason, the black dotted line shows the estimation result of kernel method applied on the 544 bubble area distribution. Obviously, the wavelet estimator has done a better job when encountering the approximation of target curves with spikes and peaks.

In Fig. 5, the bubble size mean 803 and the standard variance 627 of Fig.2(c) are used to plot the normal distribution. Apparently the bubble size distribution concerned is non-normal. Commonly used statistical characteristics like variance, kurtosis, and skewness are inaccurate features for bubble size distribution, except that mean is of value to some extent. The normal distribution described using a mean and standard deviation is, therefore, unable to accurately and fully describe the bubble size density. It is found that all the typical froth size distributions in rough cells tend to have a long tail with skewness to the left.

Corresponding to the three segmented froth images in Fig.2, Fig.6 presents the three output PDF curves that were estimated by using the wavelet threshold estimators. The green curve related to sticky and small bubble image Fig.2 (a) denotes that most bubble size are under 1500, with a peak around area 300. The blue PDF curve of Fig.2 (b) has a heavy tail extended to 7000 pixels. The red PDF curve for Fig.2 (c) shows that the number of bubbles with area under 1000 is relatively the least, while the bubbles with area between 1000 and 3000 are more than that of the ideal green curve of Fig.2(a).

A Machine Vision based froth analyzer [10] consisting of a RGB camera, a lamp and a hook is installed above the surface of froth layer in the industry field, which provides the online acquisition of froth videos and images. Real time segmentation is carried out. Dynamic tracking of size distribution reflected by segmentation results is technically detective on line. Fig.7 gives a demonstration of real time 3-D mesh plot of output PDF. Therefore, the online monitoring of operational parameter and chemical addition can be accomplished by observing the real time variance of output PDFs distribution shape. By choosing appropriate wavelet bases, size density $\gamma(x)$ is converted to description of a

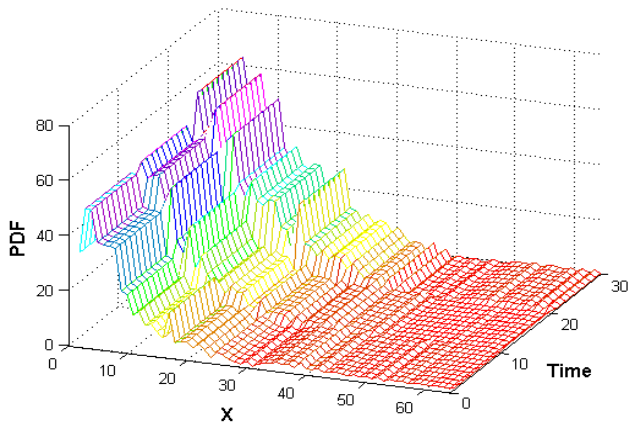

Fig.7 The 3-D mesh plot of the output PDF.

group of wavelet coefficients vectors. Define the dynamic wavelet coefficients vector as:

$$V = f(V, u(t))$$

In discrete system:

$$V_{k+1} = f(V_k, u_k)$$

where u_k is the control input of industry process. To track the output PDFs to a target distribution shape, various stochastic control approaches can be designed based on the dynamic coefficient vectors.

V. CONCLUSION

In this work, online acquisition of froth videos and images are made available by installing froth analyzer. Real time froth segmentation using watershed method is implemented in C language with a user interface. Statistic bubble size distribution is described by using non-linear wavelet threshold estimator to approximate the output PDFs. The monitoring of the process can be solved by transforming the problem of tracking output bubble size PDFs to the problem of tracking wavelet estimation coefficients vectors. Various stochastic control strategies can be designed based on the dynamic coefficient vectors to achieve a target PDF distribution shape.

REFERENCES

[1] D.W.Moolman, J.J.Eksteen, C.Aldrich, and J.S.J. van Deventer, "The significance of flotation froth appearance for machine vision control," *International Journal of Mineral Processing*, vol.48, no.3-4, pp.135-158, 1996.

[2] G. Bartolacci, P. Pelletier Jr. , J. Tessier Jr. , C. Duchensene, P. –A. Bosse, and J. Fournier, "Application of numerical image analysis to process diagnosis and physical parameter measurement in mineral processes—Part I: Flotation control based on froth textural characteristics," *Minerals Engineering*, vol.19, no.6-8, pp.734-747, 2006.

[3] J. Kaartinen, J. Hatonen, H. Hyotyniemi, and J. Miettunen, "Machine-vision-based control of zinc flotation — a case study," *Control Engineering Practice*, vol.14, no.12, pp.1455-1466, 2006.

[4] P. N. Holtham and K. K. Nguyen, "On-line analysis of froth surface in coal and mineral flotation using JKFrothCam," *International Journal of Mineral Processing*, vol.64, no.2-3, pp.163-180, 2002.

[5] E.Ventura-Medina and J.J.Cilliers, "Calculation of the specific surface area in flotation," *Minerals Engineering*, vol.13, no.3, pp.265-275, 2000.

[6] C. T. O'Connor, E. W. Randall, and C. M. Goodall, "Measurement of the effects of physical and chemical variables on bubble size," *International Journal of Mineral Processing*, vol.28, no.1-2, pp.139-149, 1990.

[7] W. Wang and L. Li, "Image analysis and computer vision for mineral froth," in Proceedings of *IEEE International Conf. on Mechatronics and Automation*, Niagara Falls, Canada, 2005, pp. 1790 -1795.

[8] G. Bonifazi, S. Serranti, F. Volpe, and R. Zuco, "Characterization of flotation froth structure and color by machine vision," *Computers and Geosciences*, vol. 27, no.9, pp.1111-1117, 2001.

[9] J. J. Liu, J. F. MacGregor, C. Duchesne, and G. Bartolacci, "Flotation froth monitoring using multiresolutional multivariate image analysis," *Minerals Engineering*, vol.18, no.1, pp.65-76, 2005.

[10] C. Yang, C. Xu, M. Mu, and K. Zhou, "Bubble size estimation using interfacial morphological information for mineral flotation process monitoring," *Transactions of Nonferrous Metals Society of China*, vol.19, no.3, pp.694-699,2009.

[11] J. J. Liu and J. F. MacGregor, "Froth-based modeling and control of flotation processes," *Minerals Engineering*, vol.21, no.9, pp.642-651, 2008.

[12] D.W.Scott, *Multivariate density estimation: theory, practice, and visualization*. John Wiley & Sons, New York, 1992.

[13] Y. M. Zhang, L. Guo, and H. Wang, "Filter based fault detection and diagnosis using output PDFs for stochastic systems with time delays," *International Journal of Adaptive Control and Signal Process*, vol.20, pp.175-194, 2006.

[14] D. R. M. Herrick, G. P. Nason, and B. W. Silverman, "Some new methods for wavelet density estimation," Technical report, Dept. Mathematics, Bristol University, 2000.

[15] M. Vannucci, "Nonparametric density estimation using wavelets," Technical report, Duke University, 1998.

[16] D. L. Donoho, I. M. Johnstone, G. Kerkyacharian, and D. Picard, "Density estimation by wavelet thresholding," *The Annals of Statistics*, vol.24, no.2, 1996.

[17] I. Daubechies, *Ten Lectures on Wavelets*. SIAM, Philadelphia, 1992.